

---

# Conditional Inference in Pre-trained Variational Autoencoders via Cross-coding

---

Ga Wu<sup>1,3</sup>, Justin Domke<sup>2</sup> and Scott Sanner<sup>1,3</sup>

<sup>1</sup>Department of Mechanical and Industrial Engineering, University of Toronto

<sup>2</sup>College of Computing and Information Sciences, University of Massachusetts

<sup>3</sup>Vector Institute

{wuga,ssanner}@mie.utoronto.ca      domke@cs.umass.edu

## Abstract

Variational Autoencoders (VAEs) are a popular generative model, but one in which conditional inference can be challenging. If the decomposition into query and evidence variables is fixed, conditional VAEs provide an attractive solution. To support arbitrary queries, one is generally reduced to Markov Chain Monte Carlo sampling methods that can suffer from long mixing times. In this paper, we propose an idea we term *cross-coding* to approximate the distribution over the latent variables after conditioning on an evidence assignment to some subset of the variables. This allows generating query samples *without* retraining the full VAE. We experimentally evaluate three variations of cross-coding showing that (i) two can be quickly trained for different decompositions of evidence and query and (ii) they quantitatively and qualitatively outperform Hamiltonian Monte Carlo.

## 1 Introduction

Variational Autoencoders (VAEs) [7] are a popular deep generative model of joint probability distributions with numerous extensions including variations for planar flow [12], inverse autoregressive flow [8], importance weighting [1], ladder networks [11], and discrete latent spaces [14] to name just a few. Unfortunately, existing methods for conditional inference in VAEs are limited. Conditional VAEs (CVAEs) [16] allow VAE training conditioned on a fixed decomposition of evidence and query, but can become computationally prohibitive to train when large numbers of queries with differing decompositions are required. Alternatively, Markov Chain Monte Carlo methods such as Hamiltonian Monte Carlo (HMC) [4, 3] are difficult to adapt to these problems, and can suffer from long mixing times as we show empirically.

To remedy the limitations of existing methods for conditional inference in VAEs, we aim to approximate the distribution over the latent variables after conditioning on an evidence assignment through a variational Bayesian methodology. In doing this, we reuse the decoder of the VAE *without* the computational expense of re-training it as done by the CVAE approach, which leads to a fortuitous cancellation in the KL-divergence that yields substantially simplified and accelerated inference. We term the network that generates the conditional latent distribution the *cross-coder*.

We experiment with two cross-coding alternatives: Gaussian variational inference via a linear transform (GVI) and Normalizing Flows (NF). We also provide some comparison to a fully connected network (FCN), which suffer from some technical and computational issues but provides a useful point of reference for experimental comparison purposes. Overall, our results show that the GVI and NF variants of cross-coding can be trained quickly for arbitrary decompositions of query and evidence and compare favorably to ground truth results provided by rejection sampling, which is only viable for low latent dimensionality. Furthermore, we observe that HMC often fails to mix

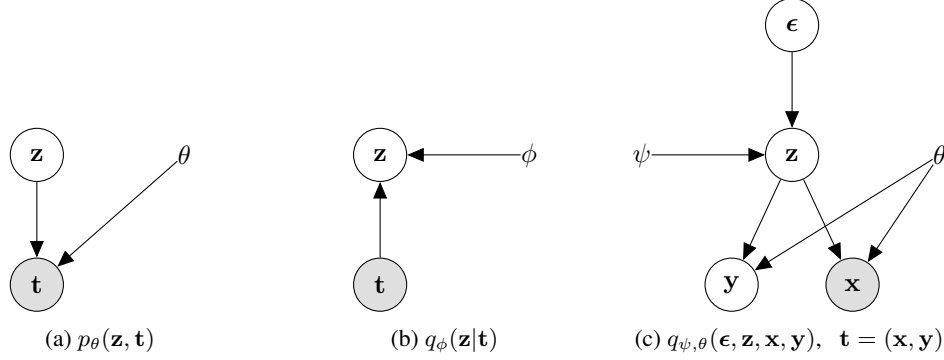


Figure 1: Graphical model of the proposed framework. (a) Decoder  $p_\theta(\mathbf{z}, \mathbf{t}) = p(\mathbf{z})p_\theta(\mathbf{t}|\mathbf{z})$ , representing the generative model. This is exactly the standard VAE model. (b) Encoder:  $q_\phi(\mathbf{z}|\mathbf{x}, \mathbf{y})$ . Since exact maximum-likelihood learning is intractable, VAE training uses this to bound the likelihood using the ELBO (Eq. 2). (c) Cross Encoder:  $q_{\psi, \theta}(\epsilon, \mathbf{z}, \mathbf{x}, \mathbf{y}) = q(\epsilon)q_\psi(\mathbf{z}|\epsilon)p_\theta(\mathbf{x}, \mathbf{y}|\mathbf{z})$ . This re-uses the decoder parameters  $\theta$ , but  $\psi$  is optimized by C-ELBO (Eq. 5). Here,  $\mathbf{t}$  is “split” as  $\mathbf{t} = (\mathbf{x}, \mathbf{y})$ .

despite systematic efforts to tune its parameters and hence demonstrates poor performance compared to cross-coding in both quantitative and qualitative evaluation.

## 2 Background

### 2.1 Variational Auto-encoder

One way to define an expressive generative model  $p_\theta(\mathbf{t})$  is to introduce latent variables  $\mathbf{z}$ . For example, Variational Auto-Encoders (VAEs) [7] model  $p(\mathbf{z})$  as a simple fixed Gaussian distribution. Then,  $p_\theta(\mathbf{t}|\mathbf{z})$  is a Gaussian for real  $\mathbf{t}$ , but with the mean determined by a “decoder” network

$$p_\theta(\mathbf{t}|\mathbf{z}) = \mathcal{N}(\mathbf{t}; \text{Decoder}_\theta(\mathbf{z}), \sigma^2 I), \quad (1)$$

or a product of independent Bernoulli’s parameterized by a sigmoidally transformed decoder if  $\mathbf{t}$  is binary. Hence the generative model of a VAE corresponds to Fig. 1(a). If the decoder network has high capacity, the marginal distribution  $p_\theta(\mathbf{t})$  can represent a wide range of distributions. In principle, one might wish to train such a model by (regularized) maximum likelihood. Unfortunately, the marginal likelihood  $p_\theta(\mathbf{t})$  is intractable. However, a classic idea is to use variational inference to lower-bound it [15]. For any distributions  $p_\theta$  and  $q_\phi$ ,

$$\log p_\theta(\mathbf{t}) = \log \int_{\mathbf{z}} p_\theta(\mathbf{t}, \mathbf{z}) d\mathbf{z} = \underbrace{\mathbb{E}_{q_\phi(\mathbf{z}|\mathbf{t})} \log \frac{p_\theta(\mathbf{Z}, \mathbf{t})}{q_\phi(\mathbf{Z}|\mathbf{t})}}_{\text{ELBO}[q_\phi(\mathbf{z}|\mathbf{t})||p_\theta(\mathbf{z}, \mathbf{t})]} + KL[q_\phi(\mathbf{Z}|\mathbf{t})||p_\theta(\mathbf{Z}|\mathbf{t})]. \quad (2)$$

Since the KL-divergence is non-negative, the “evidence lower bound” (ELBO) lower bounds  $\log p_\theta(\mathbf{t})$ . Thus, one can maximize the ELBO with respect to  $\theta$  and  $\phi$  simultaneously as a surrogate to the likelihood.

VAEs represent  $q_\phi$  as a Gaussian, with a mean and covariance both given as the output of an “encoder” network depicted in Fig. 1(b) with distribution

$$q_\phi(\mathbf{z}|\mathbf{t}) = \mathcal{N}(\mathbf{z}; \text{Encoder}_\phi(\mathbf{t})).$$

### 2.2 The conditional inference problem

In this paper, we assume a VAE has been trained. Then, at test time, after decomposing  $\mathbf{t} = (\mathbf{x}, \mathbf{y})$  and observing  $\mathbf{x}$  as evidence, one would like to infer the distribution of the non-observed  $\mathbf{y}$ . If this decomposition of  $\mathbf{t}$  into evidence and query variables is fixed and known ahead of time, a natural solution is to train an explicit conditional model, the approach taken by Conditional Variational Autoencoders[16]. We focus on supporting *arbitrary* queries, where training a conditional model for each possible decomposition  $\mathbf{t} = (\mathbf{x}, \mathbf{y})$  is infeasible.

### 3 Conditional Inference on Variational Auto-encoders

We now turn to the details of conditional inference. We assume we have pretrained a VAE (i.e.,  $\theta$  and  $\phi$  in Fig. 1 (a) and (b)) and now wish to approximate the distribution  $p_\theta(\mathbf{y}|\mathbf{x})$  where  $\mathbf{x}$  is some new “test” input not known at VAE training time. Unfortunately, exact inference is difficult, since computing this probability exactly would require marginalizing out  $\mathbf{z}$ .

#### 3.1 Exploiting Factorization in the Output

One helpful property comes from the fact that in a VAE, the conditional distribution over the output (Eq. 1) has a diagonal covariance, which leads to the following decomposition:

**Observation 1** The distribution of a VAE can be factorized as  $p_\theta(\mathbf{x}, \mathbf{y}, \mathbf{z}) = p(\mathbf{z})p_\theta(\mathbf{x}|\mathbf{z})p_\theta(\mathbf{y}|\mathbf{z})$ .

Since  $\mathbf{x}$  and  $\mathbf{y}$  are conditionally independent given  $\mathbf{z}$ , the conditional of  $\mathbf{y}$  given  $\mathbf{x}$  can be written as

$$p_\theta(\mathbf{y}|\mathbf{x}) = \int_{\mathbf{z}} p_\theta(\mathbf{z}|\mathbf{x})p_\theta(\mathbf{y}|\mathbf{z})d\mathbf{z}. \quad (3)$$

This factorization can also be exploited by Markov chain Monte Carlo methods (MCMC), such as Hamiltonian Monte Carlo (HMC) [4, 3].

In this case, it allows the Markov chain to be defined over  $\mathbf{z}$  alone, rather than  $\mathbf{z}$  and  $\mathbf{y}$  together. That is, one can use MCMC to attempt sampling from  $p_\theta(\mathbf{z}|\mathbf{x})$ , and then draw exact samples from  $p_\theta(\mathbf{y}|\mathbf{z})$  just by evaluating the decoder network at each of the samples of  $\mathbf{z}$ . The experiments using MCMC in Section 4 use this strategy.

#### 3.2 Variational Inference Bounds

The basic idea of variational inference (VI) is to posit some distribution  $q_\psi$ , and optimize  $\psi$  to make it match the target as closely as possible. So, in principle, the goal of VI would be to minimize  $KL[q_\psi(\mathbf{Y}|\mathbf{x})||p_\theta(\mathbf{Y}|\mathbf{x})]$ . For an arbitrary distribution  $q_\psi$  this divergence would be difficult to work with, again due to the need to marginalize out  $\mathbf{z}$  in  $p_\theta$ .

However, if  $q_\psi$  is chosen carefully, then the above divergence can be upper-bounded by one defined directly over  $\mathbf{Z}$ . Specifically, we will choose  $q_\psi$  so that the dependence of  $\mathbf{y}$  on  $\mathbf{z}$  under  $q_\psi$  uses the same “decoder” as in  $p_\theta$ .

**Lemma 1.** *Suppose we choose  $q_\psi(\mathbf{z}, \mathbf{y}|\mathbf{x}) = q_\psi(\mathbf{z})p_\theta(\mathbf{y}|\mathbf{z})$ . Then*

$$KL[q_\psi(\mathbf{Y}|\mathbf{x})||p_\theta(\mathbf{Y}|\mathbf{x})] \leq KL[q_\psi(\mathbf{Z}|\mathbf{x})||p_\theta(\mathbf{Z}|\mathbf{x})]. \quad (4)$$

This is proven in the Appendix. The result follows from using the chain rule of KL-divergence [2] to bound the divergence over  $\mathbf{Y}$  by the divergence jointly over  $\mathbf{Y}$  and  $\mathbf{Z}$ . Then the common factors in  $q_\psi$  and  $p_\theta$  mean this simplifies into a divergence over  $\mathbf{Z}$  alone.

Given this Lemma, it makes sense to seek a distribution  $q_\psi$  such that the divergence on the right-hand side of Eq. 4 is as low as possible. To minimize this divergence, consider the decomposition

$$\log p_\theta(\mathbf{x}) = \underbrace{\mathbb{E}_{q_\psi(\mathbf{z}|\mathbf{x})} \log \frac{p_\theta(\mathbf{Z}, \mathbf{x})}{q_\psi(\mathbf{Z}|\mathbf{x})}}_{\text{C-ELBO}[q_\psi(\mathbf{z}|\mathbf{x})||p_\theta(\mathbf{z}, \mathbf{x})]} + KL[q_\psi(\mathbf{Z}|\mathbf{x})||p_\theta(\mathbf{Z}|\mathbf{x})], \quad (5)$$

which follows from Eq. 2 by substituting  $\mathbf{t} \rightarrow \mathbf{x}$  and  $q_\phi \rightarrow q_\psi$ . Here, we call the first term the “conditional ELBO” (C-ELBO) to reflect that maximizing it is equivalent to minimizing an upper bound on the conditional divergence between  $q_\psi(\mathbf{Y}|\mathbf{x})$  and  $p_\theta(\mathbf{Y}|\mathbf{x})$ .

#### 3.3 Inference via Cross-coding

The previous section says that we should seek a distribution  $q_\psi$  to approximate  $p_\theta(\mathbf{z}|\mathbf{x})$ . Although the latent distribution  $p(\mathbf{z})$  may be simple, the conditional distribution  $p(\mathbf{z}|\mathbf{x})$  is typically complex and often multimodal (cf. Fig. 3).

We propose to draw  $\epsilon$  from some fixed base density  $q(\epsilon)$  and then use a network with parameters  $\psi$  to map to the latent space  $\mathbf{z}$ . The full variational distribution is therefore

$$q_\psi(\epsilon, \mathbf{z}, \mathbf{x}, \mathbf{y}) = q(\epsilon)q_\psi(\mathbf{z}|\epsilon)\mathbf{p}_\theta(\mathbf{x}, \mathbf{y}|\mathbf{z}) \quad \text{with} \quad \mathbf{q}_\psi(\mathbf{z}|\epsilon) = \delta(\mathbf{z} - \text{XCoder}_\psi(\epsilon)), \quad (6)$$

where  $\delta$  is a multivariate delta function. We call this network a ‘‘Cross-coder’’ to emphasize that the parameters  $\psi$  are fit so that the conditional  $q_\psi(\mathbf{Z}|\mathbf{x})$  matches  $p_\theta(\mathbf{Z}|\mathbf{x})$ , and so that  $\mathbf{z}$ , when ‘‘decoded’’ using  $\theta$ , will predict  $\mathbf{Y}$ .

**Theorem 2.** *If  $q_\psi$  as defined in Eq. 6 is one-to-one, the C-ELBO from Eq. 5 becomes*

$$\text{C-ELBO}[q_\psi(\mathbf{z}|\mathbf{x})||p_\theta(\mathbf{z}, \mathbf{x})] = \mathbb{E}_{q(\epsilon)} [\log p_\theta(\text{XCoder}_\psi(\epsilon), \mathbf{x}) + \log |\nabla \text{XCoder}_\psi(\epsilon)|] + \mathbb{H}[q(\epsilon)],$$

where  $\mathbb{H}[q(\epsilon)]$  is the (fixed) entropy of  $q(\epsilon)$ ,  $\nabla$  is the Jacobian with respect to  $\epsilon$ , and  $|\cdot|$  is the determinant.

We explore the following two candidate Cross-Coders.

**Gaussian Variational Inference (GVI):** The GVI  $\text{XCoder}_\psi$  linearly warps a spherical Gaussian over  $\epsilon$  into an arbitrary Gaussian  $\mathbf{z}$ :

$$\text{XCoder}_\psi(\epsilon) = \mathbf{W}\epsilon + \mathbf{b}, \quad \text{where} \quad \log |\nabla \text{XCoder}_\psi(\epsilon)| = \log |\mathbf{W}|, \quad (7)$$

such that  $\psi = (\mathbf{W}, \mathbf{b})$ ,  $\mathbf{W}$  is a square matrix linear transform and  $\mathbf{b}$  is the mean vector. While projected gradient descent can be used to maintain invertibility of  $W$ , we did not encounter issues with non-invertible  $W$  requiring projection during our experiments.

**Normalizing Flows (NF):** A normalizing flow [12] projects a probability density through a sequence of easy computable and invertible mappings. By stacking multiple mappings, the transformation can be complex. We use the special structured network called Planar Normalizing Flow:

$$\mathbf{h}_i = f_i(\mathbf{h}_{i-1}) = \mathbf{h}_{i-1} + \mathbf{u}_i g(\mathbf{h}_{i-1}^T \mathbf{w}_i + b_i), \quad (8)$$

for all  $i$ , where  $h_0 = \epsilon$ ,  $i$  is the layer id,  $w$  and  $u$  are vectors, and the output dimension is exactly same with the input dimension. Using  $\circ$  for function composition, the  $\text{XCoder}_\psi$  is given as

$$\text{XCoder}_\psi(\epsilon) = f_k \circ f_{k-1} \cdots f_1(\epsilon), \quad \text{where} \quad \log |\nabla \text{XCoder}_\psi(\epsilon)| = \sum_{i=1}^k \log |\nabla f_i|. \quad (9)$$

The fact that  $q_\psi$  must be one-to-one limits the bound in Theorem 2 to invertible  $\text{XCoder}_\psi$ s. Nevertheless, we find **Fully Connected Networks (FCNs)** useful for comparison in low-dimensional visualizations. Here, the Jacobian must be calculated using separate gradient calls for each output variable, and the lack of invertibility prevents the C-ELBO bound from being strict.

We summarize our approach in Algorithm 1. In brief, we define a variational distribution  $q(\epsilon, \mathbf{z}) = q(\epsilon)q_\psi(\mathbf{z}|\epsilon)$  and optimize the parameters  $\psi$  so that  $q_\psi(\mathbf{z})$  is close to  $p_\theta(\mathbf{z}|\mathbf{x})$ . The variational distribution includes a ‘‘CrossCoder’’ as  $q_\psi(\mathbf{z}|\epsilon) = \delta(\mathbf{z} - \text{XCoder}_\psi(\epsilon))$ . The algorithm uses stochastic gradient descent on the C-ELBO with gradients estimated using Monte Carlo samples of  $\epsilon$  and the reparameterization trick [7, 17, 13]. After inference, the original VAE distribution  $p_\theta(\mathbf{y}|\mathbf{z})$  is used to get samples over the query variables.

---

**Algorithm 1** Conditional Inference via Cross-coding.

---

1. Input a pre-trained VAE  $p_\theta(\mathbf{z}, \mathbf{x}, \mathbf{y}) = p(\mathbf{z})p_\theta(\mathbf{x}|\mathbf{z})p_\theta(\mathbf{y}|\mathbf{z})$ .
  2. Define the objective  $L(\psi) = \mathbb{E}_{q(\epsilon)} \log p_\theta(\mathbf{z} = \text{XCoder}_\psi(\epsilon), \mathbf{x}) + \log |\nabla \text{XCoder}_\psi(\epsilon)|$ .
  3. Maximize  $L(\psi)$  by SGD, drawing  $\epsilon \sim q(\epsilon)$  and estimating gradients via reparameterization.
  4. Draw a sample  $\{\mathbf{z}_m\}_{m=1}^M$ , with  $\mathbf{z}_m = \text{XCoder}_\psi(\epsilon_m)$ ,  $\epsilon_m \sim q(\epsilon)$ .
  5. Predict  $p_\theta(\mathbf{y}|\mathbf{x}) \approx \frac{1}{M} \sum_{m=1}^M p_\theta(\mathbf{y}|\mathbf{z}_m)$ .
-

## 4 Experiments

Having defined our cross-coding methodology for conditional inference with pre-trained VAEs, we now proceed to empirically evaluate our three previously defined XCoder instantiations and compare them with (Markov chain) Monte Carlo (MCMC) sampling approaches on three different pre-trained VAEs. Below we discuss our datasets and methodology followed by our experimental results.

### 4.1 Datasets and Pre-trained VAEs

**MNIST** is the well-known benchmark handwritten digit dataset [9]. We use a pre-trained VAE with a fully connected encoder and decoder each with one hidden layer of 64 ReLU units, a final sigmoid layer with Bernoulli likelihood, and 2 latent dimensions for  $\mathbf{z}$ .<sup>1</sup> The VAE has been trained on 60,000 black and white binary thresholded images of size  $28 \times 28$ . The limitation to 2 dimensions allows us to visualize the conditional latent distribution of all methods and compare to the ground truth through a fine-grained discretization of  $\mathbf{z}$ .

**Anime** is a dataset of animated character faces [5]. We use a pre-trained VAE with convolutional encoder and deconvolutional decoder, each with 4 layers. The decoder contains respective channel sizes (256, 128, 32, 3) each using  $5 \times 5$  filters of stride 2 and ReLU activations followed by batch norm layers. The VAE has a final tanh layer with Gaussian likelihood, and 64 latent dimensions for  $\mathbf{z}$ .<sup>2</sup> The VAE has been trained on 20000 images encoded in RGB of size  $64 \times 64 \times 3$ .

**CelebA** dataset [10] is a benchmark dataset of images of celebrity faces. We use a pre-trained VAE with a structure that exactly matches the Anime VAE provided above, except that it uses 100 latent dimensions for  $\mathbf{z}$ .<sup>3</sup> The VAE has been trained on 200,000 images encoded in RGB of size  $64 \times 64 \times 3$ .

### 4.2 Methods Compared

For sampling approaches, we evaluate rejection sampling (**RS**), which is only feasible for our MNIST VAE with a 2-dimensional latent embedding for  $\mathbf{z}$ . We also compare to the MCMC method of Hamiltonian Monte Carlo (**HMC**) [4, 3]. Both sampling methods exploit the VAE decomposition and sampling methodology described in Section 3.1.

For the cross-coding methods, we use the three XCoder variants described in Section 3.3: Gaussian Variational Inference (**GVI**), Planar Normalizing Flow (**NF**), and a Fully Connected Neural Network (**FCN**). By definition, the latent dimensionality of  $\epsilon$  must match the latent dimensionality of  $\mathbf{z}$  for each pre-trained VAE. Given evidence as described in the experiments, all cross-coders were trained as described in Algorithm 1. We could not train the FCN XCoder for conditional inference in Anime and CelebA due to the infeasibility of computing the Jacobian for the respective latent dimensionalities of these two VAEs.

### 4.3 Evaluation Methodology

We experiment with a variety of evidence sets to demonstrate the efficiency and flexibility of our cross-coding methodology for arbitrary conditional inference queries in pre-trained VAEs. All cross-coding inference takes (typically well) under 5 minutes per evidence set for all experiments running on an Intel Xeon E5-1620 v4 CPU with 4 cores, 16Gb of RAM, and an NVIDIA GTX1080 GPU.

Qualitatively, we visually examine the 2D latent distribution of  $\mathbf{z}$  conditioned on the evidence for the special case of MNIST, which has low enough latent dimensionality to enable us to obtain ground truth through discretization. For all experiments, we qualitatively assess sampled query images generated for each evidence set to assess both the coverage of the distribution and the quality of match between the query samples and the evidence, which is fixed in the displayed images.

Quantitatively, we evaluate the performance of the proposed framework and candidate inference methods through the following two metrics.

---

<sup>1</sup> <https://github.com/kvfrans/variational-autoencoder>

<sup>2</sup> [https://github.com/wuga214/IMPLEMENTATION\\_Variational-Auto-Encoder](https://github.com/wuga214/IMPLEMENTATION_Variational-Auto-Encoder)

<sup>3</sup> <https://github.com/yzwxx/vae-celebA>

**C-ELBO:** As a comparative measure of inference quality for each of the XCoder methods, we provide pairwise scatterplots of the C-ELBO as defined in 5 for a variety of different evidence sets.

**Query Marginal Likelihood:** For each conditional inference evaluation, we randomly select an image and then a subset of that image as evidence  $\mathbf{x}$  and the remaining pixels  $\mathbf{y}$  as the ground truth query assignment. Given this, we can evaluate the marginal likelihood of the query  $\mathbf{y}$  as follows:

$$\log p(\mathbf{y}) = \log E_{\mathbf{z}}[p(\mathbf{y}|\mathbf{z})]$$

#### 4.4 Conditional Inference on MNIST

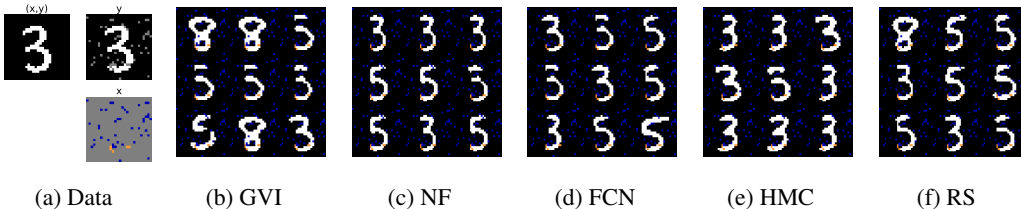


Figure 2: One conditional inference example for MNIST. In all plots, the evidence subset has white replaced with orange and black replaced with blue. (a) The original digit  $\mathbf{t}$ , the subset selected for evidence  $\mathbf{x}$ , and the remaining ground truth query  $\mathbf{y}$ . (b–f) Nine sample queries from method.

For conditional inference in MNIST, we begin with Figure 2, which shows one example of conditional inference in the pre-trained MNIST model using the different inference methods.

While the original image used to generate the evidence represents the digit 3, the evidence is very sparse allowing the plausible generation of other digits.

It is easy to see that most of the methods can handle this simple conditional inference, with only GVI producing some samples that do not match the evidence well in this VAE with 2 latent dimensions.

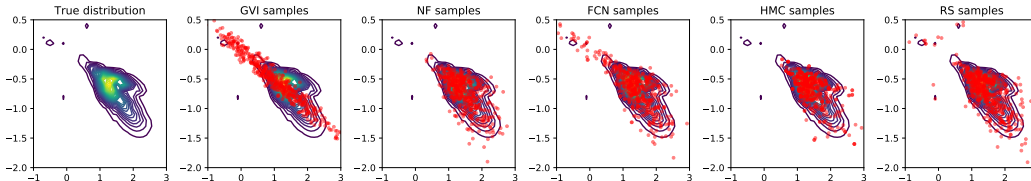


Figure 3:  $p(\mathbf{z}|\mathbf{x})$  for the MNIST example in Figure 2. The contour plot (left) shows the true distribution. The remaining plots show samples from each method overlaid on the true distribution.

To provide additional insight into Figure 2, we now turn to Figure 3, where we visually compare the true conditional latent distribution  $p(\mathbf{z}|\mathbf{x})$  (leftmost) with the corresponding distributions of each of the inference methods. At a first glance, we note that the true distribution is both multimodal and non-Gaussian. We see that GVI covers some mass not present in the true distribution that explains its relatively poor performance in Figure 2(b). All remaining methods (both XCoder and sampling) do a reasonable job of covering the irregular shape and mass of the true distribution.

We now proceed to a quantitative comparison of performance on MNIST over 50 randomly generated queries. In Figure 4(a), we present a pairwise comparison of the performance of each XCoder method on 50 randomly generated evidence sets. Noting that higher is better, we observe that FCN and NF perform comparably and generally outperform GVI. In Figure 4(b), we examine the Query Marginal Likelihood distribution for the same 50 evidence sets from (a) with each likelihood expectation generated from 500 samples. Again, noting that higher is better, here we see that RS slightly edges out all other methods with all XCoders generally performing comparably. HMC performs worst here, where we remark that inadequate coverage of the latent  $\mathbf{z}$  due to poor mixing properties leads to over-concentration on  $\mathbf{y}$  leading to a long tail in a few cases with poor coverage. We will see that these issues with HMC mixing become much more pronounced as we move to experiments in VAEs with higher latent dimensionality in the next section.

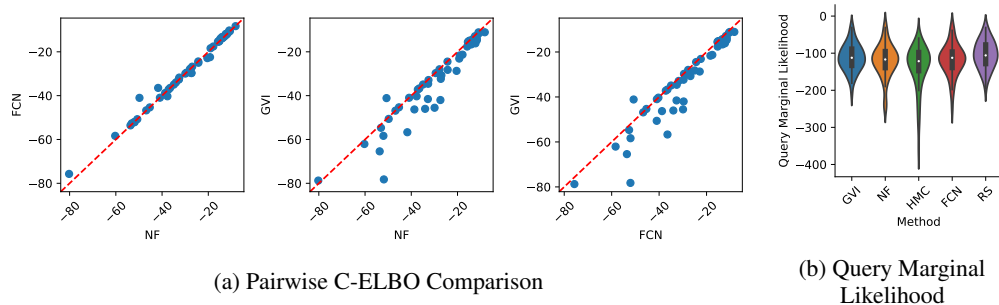


Figure 4: (a) Pairwise C-ELBO comparison of different XCoder methods evaluated over the 50 randomly generated evidence sets for MNIST. (b) Violin (distribution) plots of the Query Marginal Likelihood for the same 50 evidence sets from (a), with each likelihood expectation generated from 500 samples. For both metrics, higher is better.

#### 4.5 Conditional Inference on Anime and CelebA

Now we proceed to our larger VAEs for Anime and CelebA with respective latent dimensionality of 64 and 100 that allow us to work with larger and more visually complex RGB images. In these cases, FCN could not be applied due to the infeasibility of computing the Jacobian and RS is also infeasible for such high dimensionality. Hence, we can only compare the two XCoders GVI and NF with HMC in this section.

##### 4.5.1 Systematic HMC Tuning Analysis for Anime and CelebA

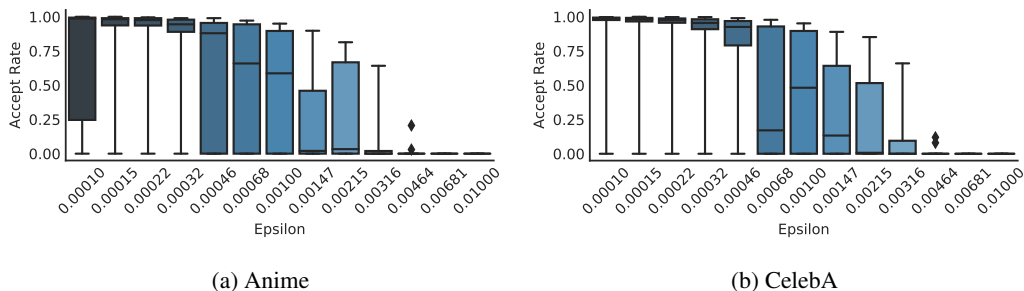


Figure 5: Boxplots of acceptance rate distribution of HMC for 30 Markov Chains vs different  $\epsilon$  on (a) Anime and (b) CelebA. Each Markov chain ran for 10,000 burn-in samples with 10 leapfrog steps per iteration.

While tuning HMC in lower dimensions was generally feasible for MNIST with a few exceptions noted in previous discussion of Figure 4(b), we observed that HMC becomes very difficult to tune in the Anime and CelebA VAEs with higher latent dimensionality. To illustrate these HMC tuning difficulties, we present a summary of our systematic efforts to tune HMC on Anime and CelebA in Figure 5 with boxplots of the acceptance rate distribution of HMC for 30 Markov Chains vs different  $\epsilon$  on (a) Anime and (b) CelebA. We ran each Markov chain for 10,000 burn-in samples with 10 leapfrog steps per iteration; we tried 3 different standard leapfrog step settings of  $\{5, 10, 30\}$ , finding that 10 leapfrog steps provided the best performance across a range of  $\epsilon$  and hence chosen for Figure 5.

In short, Figure 5 shows that only a very narrow band of  $\epsilon$  lead to a reasonable acceptance rate for good mixing properties of HMC. Even then, however, the distribution of acceptance rates for any particular Markov Chain for a good  $\epsilon$  is still highly unpredictable as given by the quartile ranges of the boxplot. In summary, we found that despite our systematic efforts to tune HMC for higher dimensional problems, it was difficult to achieve a good mixing rate and overall this leads to the generally poor performance observed for HMC on Anime and CelebA that we discuss next.

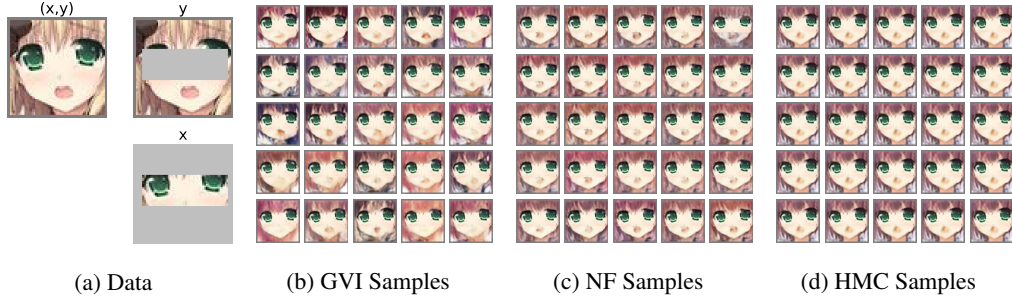


Figure 6: One conditional inference example for Anime. (a) The original image  $t$ , the subset selected for evidence  $x$ , and the remaining ground truth query  $y$ . (b–d) 25 sample queries from each method with the evidence superimposed on each image. (c,d) NF and HMC demonstrate poor coverage.

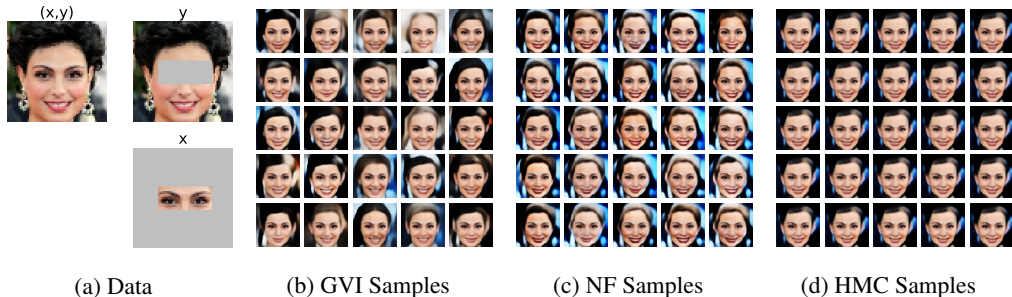


Figure 7: One conditional inference example for CelebA. (a) The original image  $t$ , the subset selected for evidence  $x$ , and the remaining ground truth query  $y$ . (b–d) 25 sample queries from each method with the evidence superimposed on each image. (d) HMC demonstrates poor coverage.

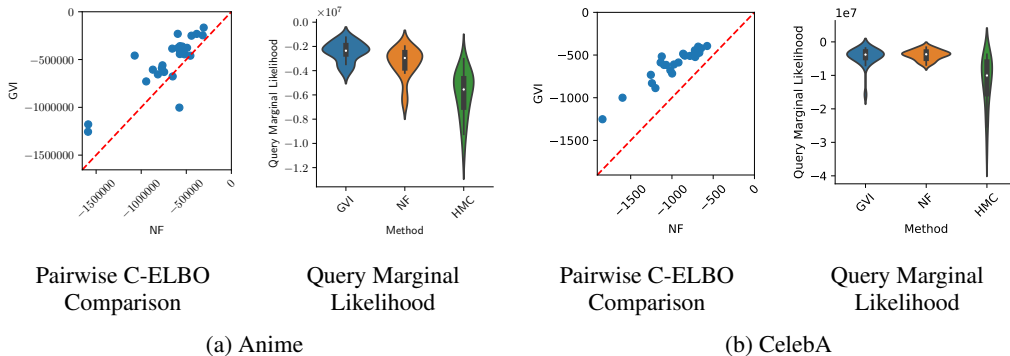


Figure 8: (left)(a,b) Pairwise C-ELBO comparison of GVI vs. FCN and (right)(a,b) Violin (distribution) plots of the Query Marginal Likelihood for (a) Anime and (b) CelebA. Evaluation details match those of Fig. 4 except with 25 conditional inference queries. For both metrics, higher is better.

#### 4.5.2 Performance Analysis for Anime and CelebA

We now proceed to a qualitative and quantitative performance analysis of conditional inference for the Anime and CelebA VAEs. Qualitatively, in Figure 6 for Anime, we see that inference for both the NF XCoder and HMC show little identifiable variation and seem to have collapsed into a single latent mode. In contrast, GVI appears to show better coverage, generating a wide range of faces that generally match very well with the superimposed evidence. For Figure 7, HMC still performs poorly, but NF appears to perform much better, with both XCoders GVI and NF generating a wide range of faces that match the superimposed evidence, with perhaps slightly more face diversity for GVI.

Quantitatively, Figure 8 strongly reflects the qualitative visual observations above. In short for the XCoders, GVI solidly outperforms NF on the C-ELBO comparison. For all methods evaluated on



Query Marginal Likelihood, GVI outperforms both NF and HMC on Anime, while for CelebA GVI performs comparably to (if not slightly worse) than NF, with both solidly outperforming HMC.

## 5 Conclusion

We introduced Cross-coding, a novel variational inference method for conditional queries in pre-trained VAEs that does not require retraining the decoder. Using three VAEs pre-trained on different datasets, we demonstrated that the Gaussian Variational Inference (GVI) and Normalizing Flows (NF) cross-coders generally outperform Hamiltonian Monte Carlo both qualitatively and quantitatively, thus providing a novel and efficient tool for conditional inference in VAEs with arbitrary queries.

## References

- [1] Yuri Burda, Roger Grosse, and Ruslan Salakhutdinov. Importance weighted autoencoders. *International Conference on Learning Representations (ICLR)*, 2016.
- [2] Thomas M Cover and Joy A Thomas. Elements of information theory 2nd edition, thm 2.5.3. 2006.
- [3] Jascha Sohl-Dickstein Daniel Levy, Matthew D. Hoffman. Generalizing hamiltonian monte carlo with neural networks. *The Sixth International Conference on Learning Representations (ICLR)*, 2018.
- [4] Mark Girolami and Ben Calderhead. Riemann manifold langevin and hamiltonian monte carlo methods. *Journal of the Royal Statistical Society: Series B (Statistical Methodology)*, 73(2): 123–214, 2011.
- [5] Yanghua Jin, Jiakai Zhang, Minjun Li, Yingtao Tian, Huachun Zhu, and Zhihao Fang. Towards the automatic anime characters creation with generative adversarial networks. *arXiv preprint arXiv:1708.05509*, 2017.
- [6] Wilfred Kaplan. *Advanced calculus*. Cambridge, Mass., Addison-Wesley Press, 1952.
- [7] Diederik P Kingma and Max Welling. Auto-encoding variational bayes. *International Conference on Learning Representations (ICLR)*, 2014.
- [8] Diederik P Kingma, Tim Salimans, Rafal Jozefowicz, Xi Chen, Ilya Sutskever, and Max Welling. Improved variational inference with inverse autoregressive flow. In *Advances in Neural Information Processing Systems (NIPS)*, pages 4743–4751, 2016.
- [9] Yann LeCun and Corinna Cortes. MNIST handwritten digit database. 2010. URL <http://yann.lecun.com/exdb/mnist/>.
- [10] Ziwei Liu, Ping Luo, Xiaogang Wang, and Xiaoou Tang. Deep learning face attributes in the wild. In *Proceedings of International Conference on Computer Vision (ICCV)*, 2015.
- [11] Lars Maaløe, Casper Kaae Sønderby, Søren Kaae Sønderby, and Ole Winther. Auxiliary deep generative models. *33rd International Conference on Machine Learning (ICML)*, 2016.
- [12] Danilo Rezende and Shakir Mohamed. Variational inference with normalizing flows. In *International Conference on Machine Learning (ICML)*, pages 1530–1538, 2015.
- [13] Danilo Jimenez Rezende, Shakir Mohamed, and Daan Wierstra. Stochastic backpropagation and approximate inference in deep generative models. In *Proceedings of the 31th International Conference on Machine Learning (ICML)*, pages 1278–1286, 2014.
- [14] Jason Tyler Rolfe. Discrete variational autoencoders. *International Conference on Learning Representations (ICLR)*, 2017.
- [15] Lawrence K. Saul, Tommi S. Jaakkola, and Michael I. Jordan. Mean field theory for sigmoid belief networks. *J. Artif. Intell. Res.*, 4:61–76, 1996.

- [16] Kihyuk Sohn, Honglak Lee, and Xinchen Yan. Learning structured output representation using deep conditional generative models. In *Advances in Neural Information Processing Systems (NIPS)*, pages 3483–3491, 2015.
- [17] Michalis K. Titsias and Miguel Lázaro-Gredilla. Doubly stochastic variational bayes for non-conjugate inference. In *Proceedings of the 31th International Conference on Machine Learning (ICML)*, pages 1971–1979, 2014.

## Appendix

### Proof

*Proof Of Lemma 1.* To show this, we first note that the joint divergence over  $\mathbf{Y}$  and  $\mathbf{Z}$  is equivalent to one over  $\mathbf{Z}$  only.

$$\begin{aligned}
 KL[q_\psi(\mathbf{Y}, \mathbf{Z}|\mathbf{x})||p_\theta(\mathbf{Y}, \mathbf{Z}|\mathbf{x})] &= KL[q_\psi(\mathbf{Z}|\mathbf{x})||p_\theta(\mathbf{Z}|\mathbf{x})] + KL[q_\psi(\mathbf{Y}|\mathbf{Z}, \mathbf{x})||p_\theta(\mathbf{Y}|\mathbf{Z}, \mathbf{x})] \\
 &\quad \text{by the chain rule of KL-divergence} \\
 &= KL[q_\psi(\mathbf{Z}|\mathbf{x})||p_\theta(\mathbf{Z}|\mathbf{x})] + KL[q_\psi(\mathbf{Y}|\mathbf{Z})||p_\theta(\mathbf{Y}|\mathbf{Z})] \\
 &\quad \text{since } \mathbf{Y} \perp \mathbf{X} | \mathbf{Z} \text{ in both } q_\psi \text{ and } p_\theta \\
 &= KL[q_\psi(\mathbf{Z}|\mathbf{x})||p_\theta(\mathbf{Z}|\mathbf{x})] \\
 &\quad \text{since } q_\psi(\mathbf{y}|\mathbf{z}) = p_\theta(\mathbf{y}|\mathbf{z})
 \end{aligned}$$

Then, the result follows just from observing (again by the chain rule of KL-divergence) that

$$KL[q_\psi(\mathbf{Y}|\mathbf{x})||p_\theta(\mathbf{Y}|\mathbf{x})] \leq KL[q_\psi(\mathbf{Y}, \mathbf{Z}|\mathbf{x})||p_\theta(\mathbf{Y}, \mathbf{Z}|\mathbf{x})].$$

□

*Proof of Theorem 2.* For the purpose of this proof, use  $c_\psi$  to denote  $\text{CrossEncoder}_\psi$ . Firstly, note that the marginal density of  $q_\psi(\mathbf{z}|\mathbf{x})$  is (via the standard formula for a change of variables [6])

$$q_\psi(\mathbf{z} = c_\psi(\epsilon)|\mathbf{x}) |\nabla c_\psi(\epsilon)| = q(\epsilon)$$

Thus, we can write

$$\begin{aligned}
 \text{C-ELBO}[q_\psi(\mathbf{z}|\mathbf{x})||p_\theta(\mathbf{z}, \mathbf{x})] &= \mathbb{E}_{q_\psi(\mathbf{z}|\mathbf{x})} \log \frac{p_\theta(\mathbf{Z}, \mathbf{x})}{q_\psi(\mathbf{Z}|\mathbf{x})} \\
 &= \mathbb{E}_{q(\epsilon)} \log \frac{p_\theta(c_\psi(\epsilon), \mathbf{x})}{q_\psi(c_\psi(\epsilon)|\mathbf{x})} \\
 &= \mathbb{E}_{q(\epsilon)} \log \frac{p_\theta(c_\psi(\epsilon), \mathbf{x})}{q(\epsilon) / |\nabla c_\psi(\epsilon)|} \\
 &= \mathbb{E}_{q(\epsilon)} [\log p_\theta(c_\psi(\epsilon), \mathbf{x}) + \log |\nabla c_\psi(\epsilon)|] + \mathbb{H}_q[\epsilon].
 \end{aligned}$$

□

### Preliminary Check of Inference Methods

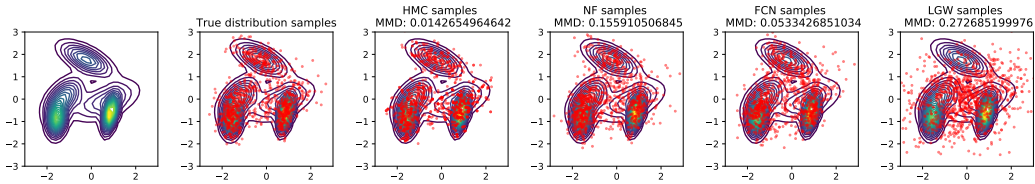


Figure 9: Comparison of different inference methods on modeling a Gaussian mixture model distribution. The true distribution samples are directly sampled from a Gaussian mixture model. Maximum mean discrepancy (MMD) values given in the plot titles are generated relative to the true sample distribution.

In this experiment, we do not use a VAE, but instead simply model a complex latent 2D multimodal distribution over  $\mathbf{z}$  as a Gaussian mixture model to evaluate the ability of each conditional inference method to accurately draw samples from this complex distribution. In general, Figure 9 shows that while the XCoders NF and FCN work well here, GVI (by definition) cannot model this multimodal distribution and HMC draws too few samples from the disconnected mode compared to the true sample distribution, indicating slight failure to mix well.

## Quality of the Pre-trained VAE Models

To assess the quality of the pre-trained VAE models, we show 100 samples from each in Figure 10.

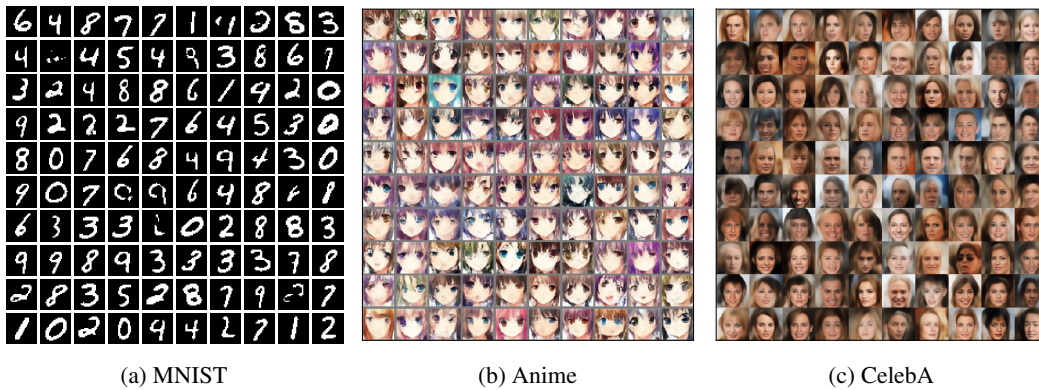


Figure 10: Samples from each of the pre-trained VAE models.

## More Inference Examples

In Figures 11 and 12, we show two additional examples of conditional inference matching the structure of experiments shown in Figures 6 and 7 in the main text. Overall, we observe the same general trends as discussed in the main text for Figures 6 and 7.

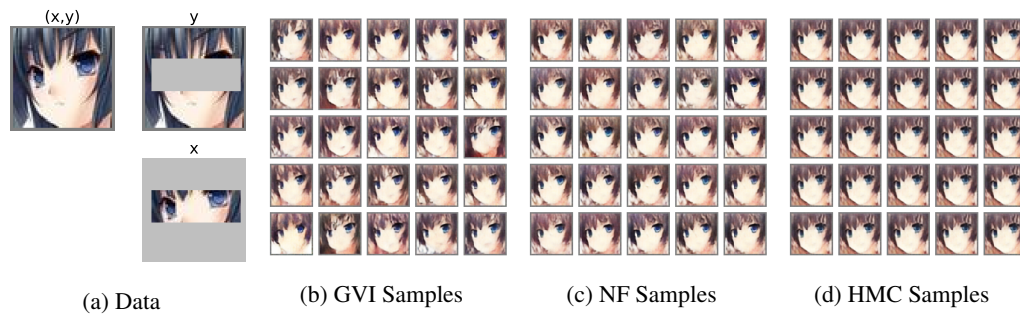


Figure 11: Another conditional inference example on Anime dataset

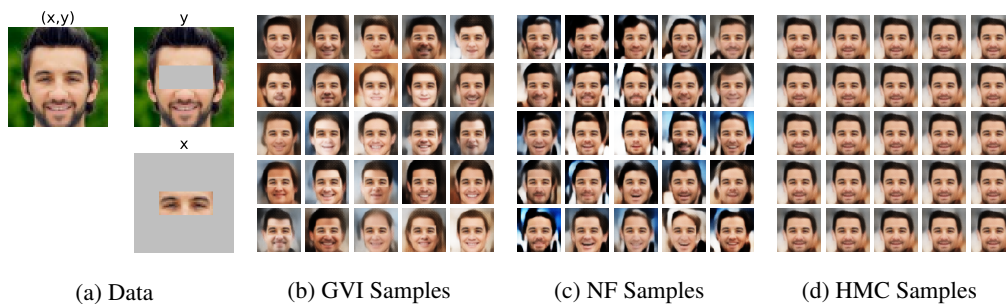


Figure 12: Another conditional inference example on CelebA dataset.

## Model Structure

In Figure 13, we show the network structure of the cross-coding conditional inference method.

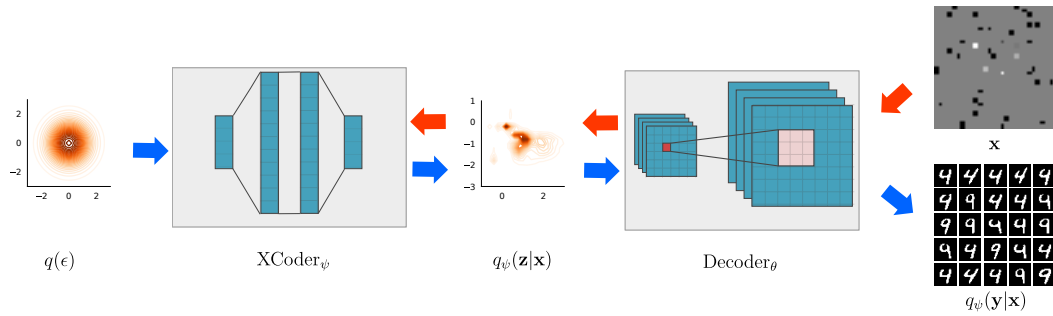


Figure 13: Framework of conditional inference on variational auto-encoder.  $\text{XCoder}_\psi$  network is distribution shifting function that we want to learn.  $\text{Decoder}_\theta$  network is extracted from pre-trained VAE model and its parameter  $\theta$  remains fixed. Red arrows indicate back-propagation(learning) flow, and blue arrows indicate forward-propagation(prediction) flow.

## Code Github Repository

[https://github.com/wuga214/XCoder\\_VAE\\_Conditional\\_Inference](https://github.com/wuga214/XCoder_VAE_Conditional_Inference)